Effects of thermal treatment on physical and mechanical properties of Valdieri Marble - NW Italy

Original
Effects of thermal treatment on physical and mechanical properties of Valdieri Marble - NW Italy / Vagnon, F.; Colombero, C.; Colombo, F.; Comina, C.; Ferrero, A. M.; Mandrone, G.; Vinciguerra, S. C.. - In: INTERNATIONAL JOURNAL OF ROCK MECHANICS AND MINING SCIENCES. - ISSN 1365-1609. - ELETTRONICO. - 116:(2019), pp. 75-86. [10.1016/j.ijrmms.2019.03.006]

Availability:
This version is available at: 11583/2742629 since: 2019-07-17T18:46:51Z

Publisher:
Elsevier Ltd

Published
DOI:10.1016/j.ijrmms.2019.03.006

Effects of Thermal Treatment on Physical and Mechanical Properties of Valdieri Marble - NW Italy

Federico Vagnon, Department of Earth Sciences, Università di Torino, Torino, 10125, Italy, federico.vagnon@unito.it (corresponding author)

Chiara Colombero, Department of Environment, Land and Infrastructure Engineering, Politecnico di Torino, Torino, 10129, Italy, chiara.colombero@polito.it

Fabrizio Colombo, Principal consultant – Ultra Petrography & Geosciences Inc., Canada, fab.petrologic@gmail.com

Cesare Comina, Department of Earth Sciences, Università di Torino, Torino, 10125, Italy, cesare.comina@unito.it

Anna Maria Ferrero, Department of Earth Sciences, Università di Torino, Torino, 10125, Italy, anna.ferrero@unito.it

Giuseppe Mandrone, Department of Earth Sciences, Università di Torino, Torino, 10125, Italy, giuseppe.mandrone@unito.it

Sergio Carmelo Vinciguerra, Department of Earth Sciences, Università di Torino, Torino, 10125, Italy, sergiocarmelo.vinciguerra@unito.it

Abstract

The effect of high temperatures as a degrading factor of rock materials is investigated in this study. Valdieri Marble samples, collected in a quarry in North-western Italian Alps, were subjected to thermal cycles (ranging from 105° to 600° C) and to subsequent non-destructive and destructive laboratory tests with the aim of evaluating the variation of physical and mechanical properties as a function of temperature variations. Physical and mechanical measurements were complemented with microscopic observations on thin sections. The increase of crack density with temperature and the consequent porosity increases were found to be the main causes of the degradation of physical and mechanical properties.

In general, density, ultrasonic pulse velocity, wet electrical resistivity, uniaxial compressive strength and Young's moduli decrease as temperature increases. By contrast, peak strain and porosity increase. Correlations between temperature and physical-mechanical properties were proposed and compared to other relationships already established in scientific literature. A damage parameter to quantify the degradation of mechanical properties with temperature is also proposed.

Keywords

Valdieri Marble; thermal treatment; mechanical and physical properties; micro-cracks.

1. Introduction

The overall physical and mechanical behaviour of upper crustal rocks is given by the combination of their geological formation and the mechanical and thermal stresses acting over time [1]. While mechanical effects have been widely investigated, less attention has been spent to the effect of temperature, which is a main mechanism of degradation and weakening of rocks. In natural volcanic and geothermal environments, high temperature gradients induced by rapid magmatic/supercritical fluid injections can induce permanent changes to the hosting material, via mineralogical transition and hydrothermal alteration, eventually enhancing potential flank collapses [2]. Similarly, in many rock-engineering applications, such as drilling, deep petroleum boring, geothermal energy exploitation, nuclear waste disposal, CO_2 storage etc., the effect of high temperatures on the mechanical properties of the materials is to be considered for a safe and successful design. Last but not least, an important field in which the effect of high temperatures on rocks plays a fundamental role is the maintenance/repair of stone-built heritage damaged by fire [3-6].

Mechanically, the effect of elevated temperatures on rocks is controlled by several parameters, among which grain size, porosity and strain rate are the most sensitive ones [7].

Two main degradation mechanisms are usually attributed to rock samples exposed to a significant temperature gradient. The first one is the propagation of pre-existing cracks, or the development of new ones, driven by thermal expansion, following the anisotropy in thermal properties of the different constituting minerals (intergranular cracks). The second mechanism is the development of micro- to macro-cracks within grains (intragranular cracks), when the minerals undergo a phase transition, mechanically enhanced by the formation of cavities due to rapid degassing or volume changes [8]. A quantitative estimation of the damage amount and a precise knowledge of its evolution and influence on the mechanical properties of the rocks exposed to heating has been only recently addressed.

In the last decades, few researches have been conducted for improving the knowledge on the mechanical behaviour of rocks affected by temperature exposure. Different rock types have been tested, among them granite [8-18], carbonatic rocks [19-24], salt [25] and sandstone [26-28]. Generally, for rocks tested under their melting point, it has been observed that mechanical and physical properties change significantly following temperature increase, demonstrating a strong dependence on this parameter.

Even if the previous findings cannot be strictly generalized since the physical and mechanical behaviours, after exposure to heating, depend on the specific mineral composition, grain size, pre-existing crack damage of the chosen rocks, for all previous studies [8-28] two main trends can be highlighted:

- In carbonatic rocks, salt and sandstone, for temperatures up to 200-300°C, mechanical properties show a moderate increase of strength with temperature, due to dilatant effects generated by thermal expansion, which result in ‘hardening’ of the bulk volume and sealing of microcracks. This is mirrored by no clear increase in micro-cracks after thermal treatment and consequent no evident changes in porosity and density. For granite, this behaviour is shifted at temperature up to 500-600°C [29].
- Generally, for temperatures higher than 400-600°C, a significant thermal damage is observed, with a progressive reduction of mechanical properties and an increase in porosity. This has been related to an increase in crack density observed with microscopic analyses. These effects are much more pronounced in carbonate rocks where at temperatures between 560°C and 800°C decarbonization occurs [2, 30].

Among the available laboratory tests, the physical and mechanical properties of rocks exposed to heating can be evaluated by either performing mechanical tests in controlled high-temperature conditions reproducing in-situ thermal constraints [9-10, 25-26, 31], or carrying out comparative measurements before and after the thermal treatment (pre- and post-heating) [19]. If adequate confining pressure is applied with temperature, the first methods may allow for a simulation of specific site conditions at depth (i.e. volcanic edifices or geothermal reservoirs). Complex testing apparatus are however needed and sensors are usually limited in number and designed to operate away from the hottest zone, so that measurements may result inaccurate. The second test methodology, in which samples are firstly subjected to a thermal cycle and then tested at room temperature conditions, allow for a separated analysis of the effects of each treatment within a cycle of heating and cooling and can take advantage of a much denser array of sensors, thus significantly improving the reliability of the measurements. The purpose of this paper is to investigate the evolution of physical and mechanical properties of a marble rock type after different thermal treatments. Marble is natural stone extensively used during ancient times in many archaeological sites and nowadays it is still attractive for building purposes. Moreover, its worldwide diffusion makes it involved in many engineering applications such as geothermal energy extraction and deep drilling. In all these cases, it can be exposed to temperature gradient and consequently, the knowledge related to the evolution of its physical and mechanical features become fundamental. Porosity, ultrasonic pulse velocity (UPV), electrical resistivity (ER) and UCS were measured on core samples treated with thermal cycles from 105°C up to 600°C. Moreover, microscopic observations were performed on thin sections of cores subjected to the same thermal cycles. Correlations between destructive and non-destructive tests as a function of temperature were observed and deeply analysed also in correlation with the observed micro-cracking patterns.

2. Material and Methods

2.1 Description of rock samples and heating procedure

Tested samples were collected in the Carbocalcio quarry (Figure 1) in the North-Western Italian Alps (Valdieri Municipality, Southern Piedmont Region) where extremely pure calcium carbonate is extracted, treated and selected for sale as granulated and micronized. In this area, the outcrops belong to the Middle Jurassic–Lower Cretaceous Provençal succession placed at the North-Eastern side of the Argentera Massif (Figure 1c) in the Western Alps [32-33].

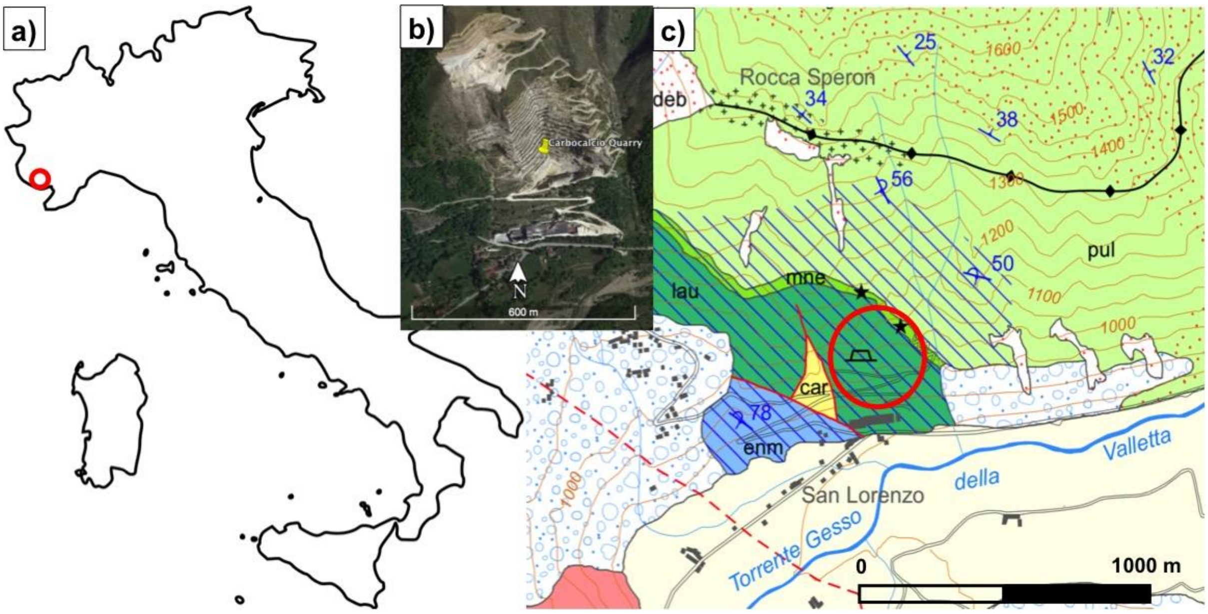

Figure 1: (a) Location, (b) satellite view and (c) geological sketch (after [30]) of the study area (red circle). Keys: enm: dark marls, calcareous marls and shales; lau: fine-grained limestones (lausa Limestone); mne: dark

shales and marls; pul: alternation of limestones and marly limestones; blue circle: glacial deposits; pale yellow: alluvial deposits; blue lines: Valdieri marble.

The main known characteristics of the tested rock type are listed in Table 1.

Table 1: Mean physical and mechanical characteristic and mineralogical composition of the studied marble.

Physical and mechanical characteristics	
Parameter	Mean value
Dry density [kg/m^3]	2720
Wet density [kg/m^3]	2740
Peak friction angle [°]	45
Residual friction angle [°]	39
Peak coesion [kPa]	96
Residual coesion [kPa]	75
Uniaxial Compressive Strenght [MPa]	115
Elastic modulus [GPa]	150
P-wave velocity [m/s]	7500
S-wave velocity [m/s]	4170
Dry apparent resistivity [Ohm m]	15800
Wet apparent resistivity [Ohm m]	12000
Porosity [-]	0.15
Mineralogical composition	
Calcite	99.90%
Quartz	>0.1%

The carbonatic rock mass (Lausa limestone) consists in fine-grained limestone, with abundant decimeter-thick beds of polymictic breccias, generally clast-supported, with millimeter to decimeter sized clasts of mudstones, coarsely crystalline dolostones and finely crystalline dolostones. Lausa limestones are followed by grey mudstones and crinoid-rich wackestones, in centimeter to decimetre thick beds, with abundant silicified portions. Fault rocks (carnieules), extremely deformed dark-coloured schists and finely bedded grey marbles with dark-grey levels are also present near the extracted white marble.

Carbonates are locally affected by a diffuse hydrothermal dolomitization occurred in the Early Cretaceous, at a very shallow burial depth, and was related to the expulsion of hot fluids (about 200°C) through faults and fractures during episodes of fault activity. Samples for this study collected within this carbonatic formation can be therefore considered as belonging to the Valdieri Marbles according to [3].

The mechanical and physical properties of eleven core specimens collected, with a diameter of 50 mm and a length of 100 mm, were measured in the laboratory in natural and after-heating conditions. To ensure samples homogeneity and representativeness, the specimens were drilled from a single rock block with approximate dimensions of 0.8x0.5x0.4 m^3.

A weak anisotropy parallel to bedding, due to a preferential orientation of microcrystalline calcite grains, has been observed for the block. This bedding has been confirmed on the tested block by several ultrasonic pulse velocity (UPV) measurements performed along three perpendicular directions of the block. Averaged UPVs measured parallel and perpendicular to the bedding were of 7500 m/s and 7000 m/s respectively, underling the weak anisotropy of the studied rock. The cylindrical core drilling was performed perpendicular to this bedding. Most of the samples show indeed a weak horizontal layering (Figure 2a).

The eleven specimens extracted from the block were grouped into four sets (Figure 2a). Each set was composed of three core samples (except one with only two specimens), in order to have a repeatability of the measurements, and was subjected to a comparable thermal treatment but reaching different target temperatures. Target temperatures of 105°C (T105), 200°C (T200), 400°C (T400) and 600°C (T600) were reached for the different sets (Figure 2b). Each thermal cycle was composed of three stages (Figure 1b): firstly, the samples were heated in a furnace at a heating rate of 0.06°C/s. Secondly, once the target temperature was reached, the specimens were held in the furnace for 24 h. Finally, in order to avoid thermal shocks, the specimens were cooled down to room temperature in the furnace. Before and after the thermal treatment, all mechanical and physical properties were measured and later compared. Standard deviations of the measured and calculated parameters values have been also evaluated following the error propagation law.

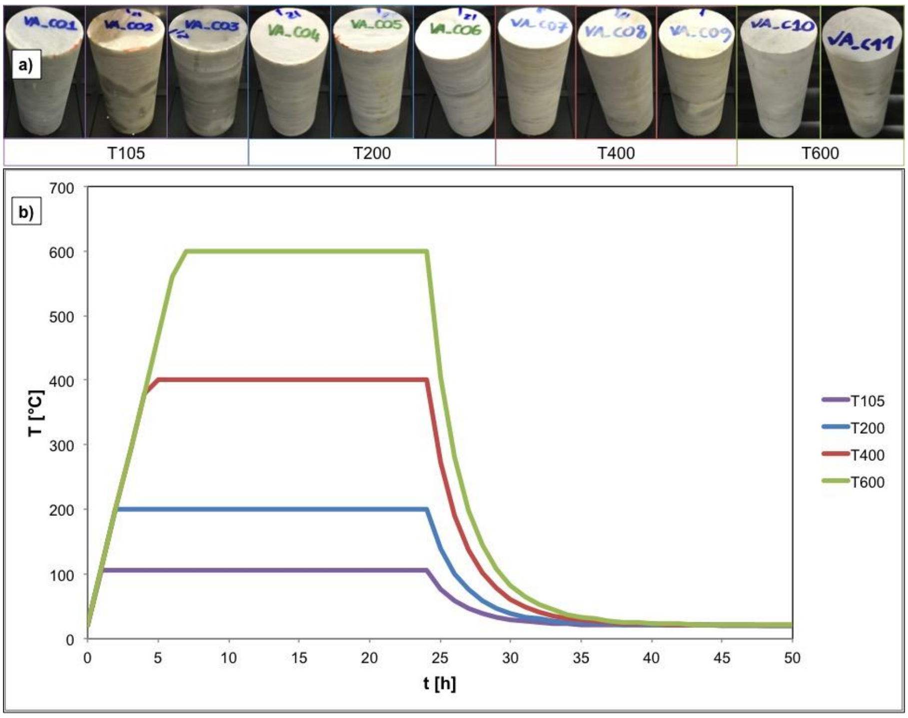

Figure 2: (a) Picture of the different sets of the marble specimens after heating to different temperatures and (b) scheme of the thermal treatment cycles followed by each sample set.

2.2 Density and porosity determination

The measurement of physical properties such as density, ρ, and porosity, n, is a good index of the degree of damage induced in the rock specimens after thermal treatment [19,20].

Since the tested specimens have a regular geometry and they are non-friable and coherent rocks, density and porosity were determined following the “Suggested methods for porosity/density determination using saturation and caliper techniques” of ISRM [34]. With this aim, the bulk volume, V, of each specimen was calculated from an average of several caliper readings along each dimension. The specimens were then saturated by water immersion and repeated shaking (for removing trapped air) for 24 h. The saturated-surface-dry mass, M_{sat}, was then determined by drying the surface with a moistened cloth, taking care to remove only surface water, and weighting the samples. The grain mass, M_s, was evaluated after a drying process in oven, at constant temperature of 105°C for 24 h.

Porosity and density (in dry, ρ_{dry}, and saturated, ρ_{wet}, sample conditions) were obtained following:

$$\rho_{dry} = \frac{\mathrm{M_S}}{V} \quad (1)$$

$$\rho_{wet} = \frac{M_{sat}}{V} \quad (2)$$

$$n = \frac{100V_v}{V}\% \quad (3)$$

where V_v is the void volume:

$$V_v = \frac{M_{sat}-M_S}{\rho_w} \quad (4)$$

2.3 UPV measurements

UPV measurements were performed using an ultrasonic pulse generation and acquisition system (Pundit Lab, Proceq). Two 54-kHz point-source (exponentially shaped) transmitter-receiver (tx-rx) transducers were used for P-wave (V_P) measurements, along the axial direction of each core sample. Cylindrical 250-kHz tx-rx probes were instead employed for S-wave (V_S) determination, along the same core direction. Measurements were conducted following ASTM D2845-08 standard requirements [35]. For each sample, 20 ultrasonic traces were recorded, using a sampling frequency of 2 MHz. Manual picking of the first arrival times was performed. Determination of the P- and S- wave ultrasonic velocity was then straightforward as the longitudinal dimension of each sample was previously measured. The representative velocity of each sample was chosen as the average of the 20 measurements.

From the V_P/V_S ratio and the determined density values, Young's, E, and shear, G, moduli and Poisson's ratio, v, were calculated for each specimen. These mechanical parameters refer to low-strain conditions and will be compared with those obtained from the first deformation phase of UCS tests.

2.4 ER measurements

ER measurements were carried out with an on-purpose built measuring quadrupole connected to a Syscal-Pro (Iris instruments) acquisition system. The instrumentation consisted of a rubber jacket with four steel electrodes (2-mm diameter and 40-mm length), disposed at the edges of two perpendicular diameters of the core sample at half of its longitudinal length (Figure 3a). Electrical measurements were performed with current injection between two subsequent electrodes (A and B, in Figure 3b) and measuring the resulting electric potential difference between the remaining couple of electrodes (M and N, in Figure 3b). The current and potential electrodes were progressively reversed and rotated around the sample, for a total of 8 different potential measurements.

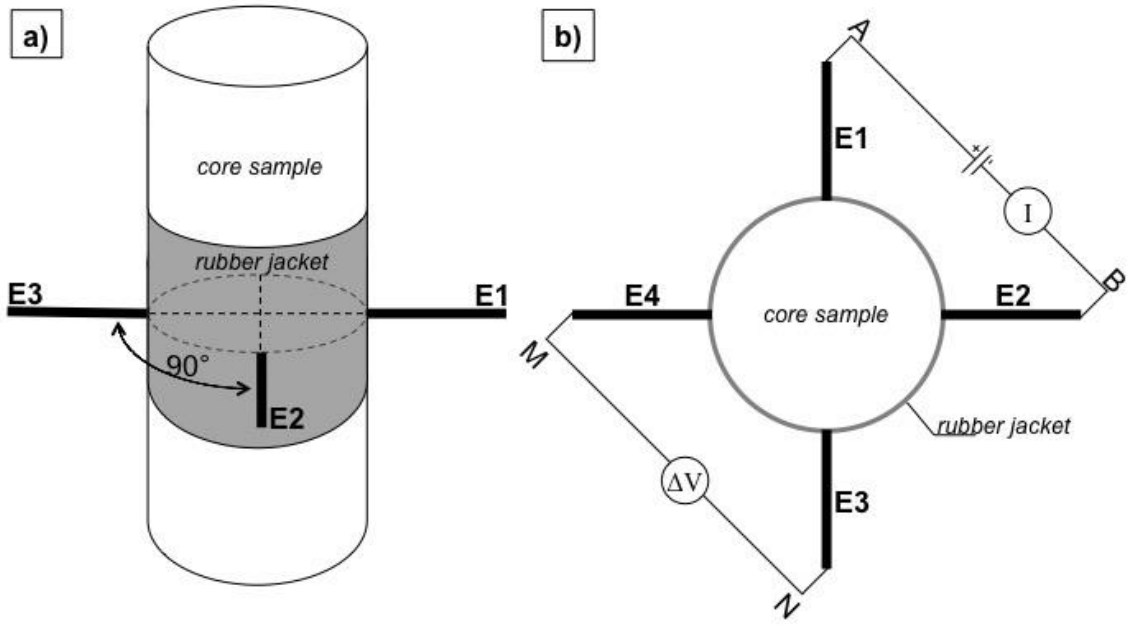

Figure 3: (a) Longitudinal view and (b) planar section of the electrical resistivity testing apparatus. E1 to E4: steel electrodes. A and B: current electrodes. M and N: potential electrodes.

The sequence was repeated three times on each sample, to obtain stable and repeatable results. From the ratio between the measured electric potential difference, ΔV_{MN}, and the injected current, I_{AB}, the determination of the sample apparent resistivity, ρ_a, follows:

$$\rho_a = k\,\frac{\Delta V_{MN}}{I_{AB}} \quad (5)$$

where k is a geometric factor, depending on the geometry of the adopted quadrupole. For the adopted array configuration, k was determined empirically by measuring the apparent resistivity of three water solutions (ρ_{w1}=5 Ωm, ρ_{w2}=10 Ωm, ρ_{w3}=23 Ωm) in four plastic cylinders with variable diameter (d_1=40 mm, d_2=65 mm, d_3=88 mm, d_4=102 mm) with the described acquisition sequence. A constant diameter-normalized k value of:

$$k = 1.24\pi d \quad (6)$$

where d is the diameter of the sample, was found from the calibration procedure. This empirical determination is in agreement with the experiments and numerical simulations of [36]. The resulting 24 apparent resistivity measurements for each sample were averaged. Each sample was tested in both dry and saturated (wet) conditions. The saturated conditions were reached leaving the sample in a saline solution (with electrical conductivity equals to 1000 µS/cm) for 24 h, with the aim of lowering the contact resistance between the electrodes and the sample surface and allowing for more stable measurements. This practice is universally recognized in ER measurements, particularly when rock materials are involved due to the high surface contact resistance (more than 1000 Ωm).

2.5 UCS tests

Mechanical properties were directly determined performing Uniaxial Compressive Strength (UCS) tests. The tests were conducted using a MTS apparatus (MTS System Corporation) equipped with a load cell of 250 kN, at a constant strain rate of 1 µm/s, following the "Suggested methods for determining the Uniaxial Compressive Strength and Deformability of Rock Materials" of ISRM [37]. Axial strain, ε_a, and diametric strain, ε_d, were measured using electrical resistance strain gauges. The axial strain was defined as the mean value of the local strains measured by two axial strain gauges, diametrically mounted along the specimen.
Uniaxial Compressive Strength, σ_u, Young's modulus, E (tangent, E_t, average, E_{av}, and secant, E_s), Poisson's ratio, ν, and shear modulus, G, were evaluated for each specimen.

2.6 Microscopic observations

The microscopic effects of thermal treatment were observed using a transmitted polarized light microscope. These analyses have the function of studying the widening and contraction of pre-existing cracks and the development of new ones after thermal treatment.
Eight thin sections, two for each target temperature, were prepared: one perpendicular (⊥) and one parallel (||) to the sample bedding. These thin sections were not directly obtained from the tested core samples (to avoid disturbances induced by destructive tests), but from additional specimens subjected to the same thermal cycles, remaining form core resizing.

3. Results and Discussion

3.1 Density and porosity determination

Both density and porosity were evaluated firstly for each sample (Figures 4a and 4c) and then as an average over the samples subjected to the same thermal treatment (sample classes from T105 to T600, Figures 4b and 4d). Variations in density (dry, ρ_{dry}, and saturated (wet), ρ_{wet}) and porosity, *n*, were observed, as shown in Figure 4. Analysing the results for each set of specimens (Figures 4a and 4c), low deviation from mean values has been observed: this aspect supports the hypothesis of homogeneity of material and it justifies the relative small number of specimens.

In general, the dry density of the specimens remains constant for temperature up to 400°C (with a slight increase at T = 400°C), after which it undergoes a significant decrease (red symbols in Figures 4a and 4b). The values of ρ_{wet} follow the same trend of ρ_{dry}, but showing a progressive divergence from dry values (blue symbols in Figure 4a and 4b).

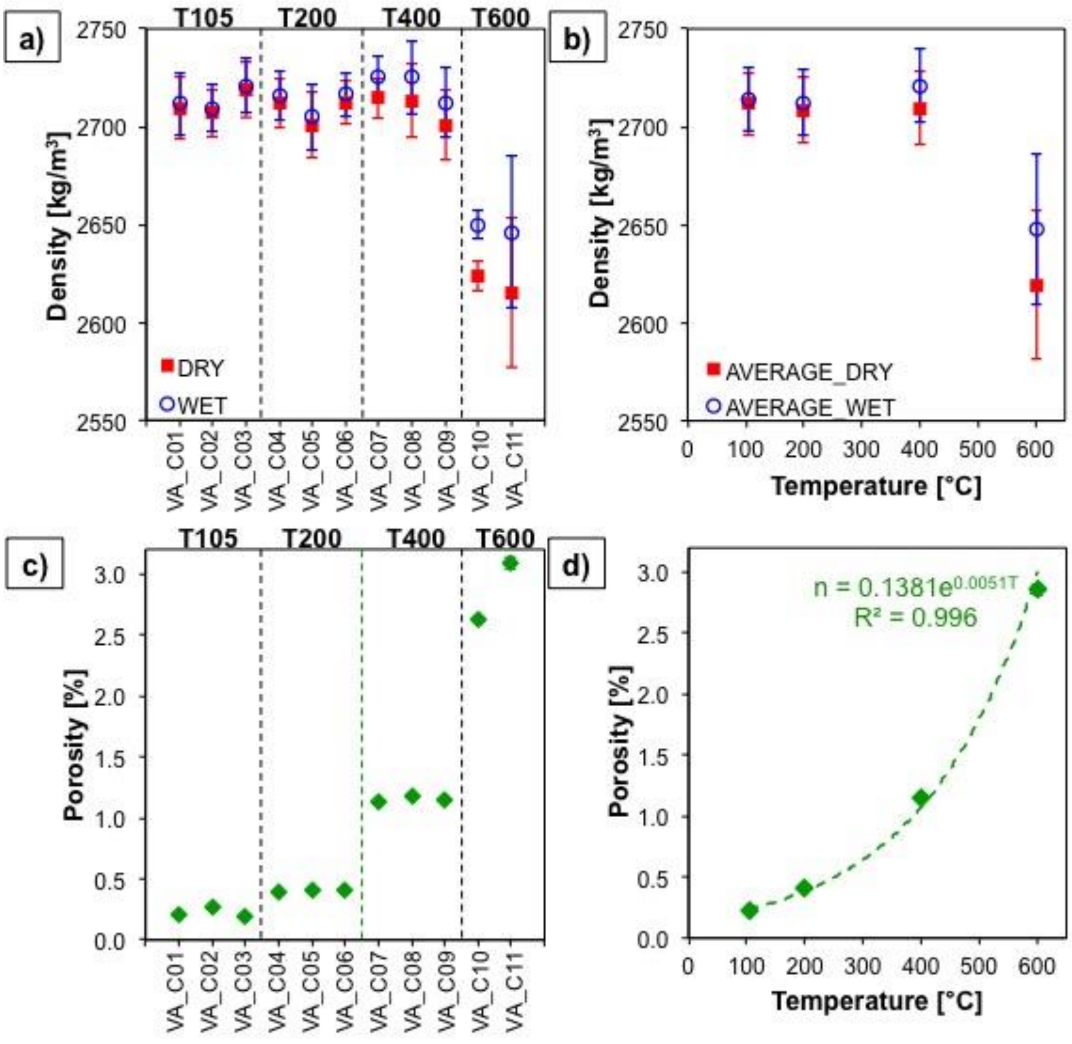

Figure 4: (a) Dry (red symbols) and wet (blue symbols) density evaluated for each sample. (b) Average dry (red symbols) and wet (blue symbols) density of each sample class (T105 to T600) as a function of the target temperature. (c) Porosity values for each sample after thermal treatment. (d) Relationship between the average porosity of each sample class and temperature. Where not visible, the dimensions of the error bars are lower than the marker size.

This behaviour appears to be caused by the thermal expansion originated by the thermal treatment, which induces internal damage because of grain crushing and micro-crack formation and/or propagation that cause a rock pore volume increase and a density decrease. The presence of water is likely to act as an inhibiting factor, slightly reducing the brittle ongoing processes and thus determining slightly higher values. This hypothesis is confirmed by analysing sample porosity, graphed as a function of temperature (Figures 4c and 4d). After the thermal cycle, there is an increase in porosity that is moderate for temperatures up to 200°C and becomes more marked for higher temperatures. In the tested temperature range (from 105 to 600°C), the porosity rises from 0.2% to 3%, with a clear exponential increase after 200°C (porosity is still about 0.4% at this temperature) and a sharp increase after 400°C (from about 1% to 3%). This well agrees with the onset of calcite decomposition which occurs at around 560°C [30] and speeds up the micro-cracking mechanisms by phase transitions inducing rapid volume changes and extra void formations. By regression analysis, we obtain the characteristic exponential relationship from our experimental data by interpolating porosity and temperature, as follow:

$$n = 0.1381e^{0.0051T} \quad (7)$$

where n is given in percentage. The goodness of this relationship is represented by the high value (0.996) of the coefficient of determination, R^2.

3.2 UPV measurements

A clear decrease in the UPV was found with increasing target temperature of the thermal treatment, as shown in Figure 5, both for P- and S-wave measurements. In general, samples treated at the same target temperature exhibited quite stable P- and S- wave velocity values (Figure 5a). The V_P/V_S ratio was found to reduce with increasing temperature. Two exponential relationships were fitted to the average velocities of each class (T105 to T600), following:

$$V_P = 9673.4e^{-0.003T} \quad (8)$$

$$V_S = 5493.7e^{-0.003T} \quad (9)$$

The two relationships (Figure 5b) show very high R^2 values, 0.981 and 0.997 respectively. These results are also in good agreement with the increase in porosity observed and the damage within the medium because of thermal cracking, which progressively slows the ultrasonic wave first arrival time at each step of temperature. In addition, since the V_P/V_S ratio is directly related to the sample Poisson’s ratio, a clear change in the mechanical properties of the samples is expected with increasing temperature. Particularly, lower V_P/V_S ratios corresponds to lower Poisson's ratios. The reduced distance of the two curves in Figure 5b suggest therefore an exponential lowering of the Poisson's ratio of the material as a function of increasing temperature, mirroring the incremental damage due to cracks formation and eventually to calcite decomposition, which provides the lowest detected V_P/V_S ratios.

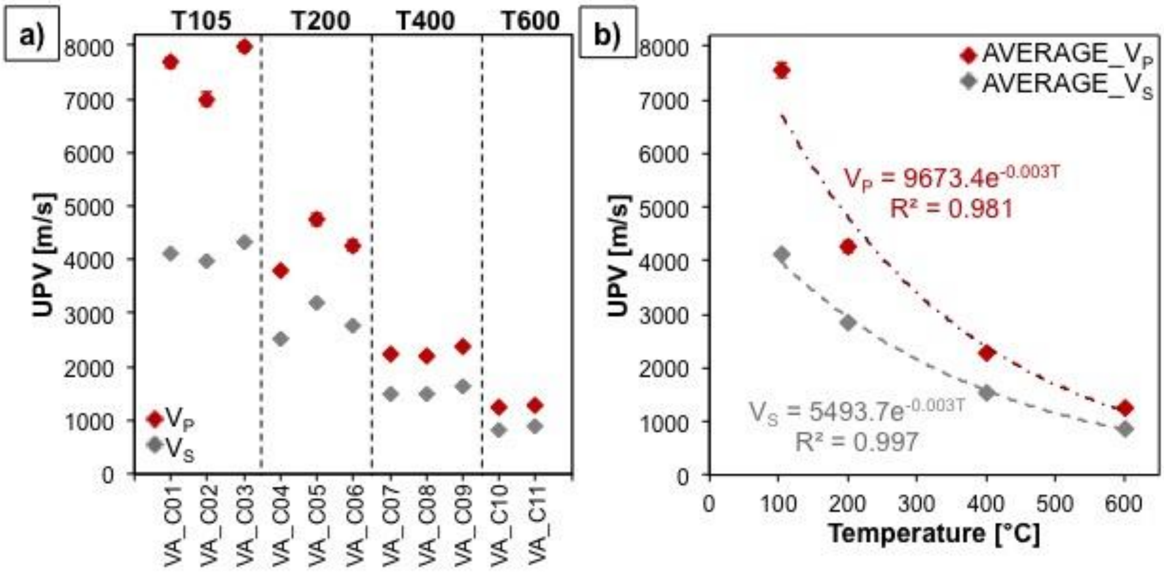

Figure 5: (a) P-wave (red symbols) and S-wave (light blue symbols) ultrasonic pulse velocities measured along the axial direction of each sample. (b) Relationships between the average P- and S-wave velocity of each sample class (T105 to T600) and the target temperature. Where not visible, the dimensions of the error bars are lower than the marker size.

3.3 ER measurements

ER values measured on the same samples are summarized in Figure 6, both for dry ($\rho_{a,dry}$) and wet ($\rho_{a,wet}$) test conditions. As shown in Figure 6a, ER values are quite stable among the samples threated to the same target temperature. Conversely, a clear modification in the electrical properties is found between the different classes. In particular, $\rho_{a,dry}$ values are found to slightly increase with increasing temperatures, while a clear decrease in $\rho_{a,wet}$ values is noticed. For electrical resistivity measured both in dry and wet conditions, the best fitting for the average values of the four classes is provided by exponential relationships (Figure 6b), following:

$$\rho_{a,dry} = 15470e^{0.0013T} \qquad (10)$$

$$\rho_{a,wet} = 14047e^{-0.0090T} \qquad (11)$$

Both relationships have very high R^2 values of 0.906 and 0.953 respectively.

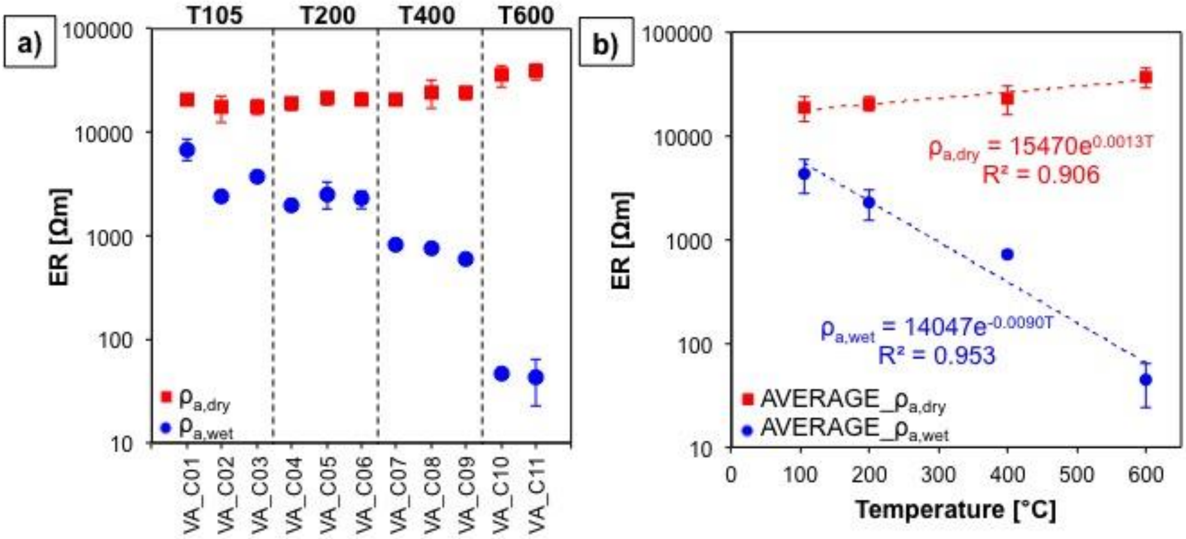

Figure 6: (a) Dry (red symbols) and wet (blue symbols) electrical resistivity values measured on each sample. (b) Relationships between the average dry and wet average electrical resistivities of each sample class (T105 to T600) and the target temperature. Where not visible, the dimensions of the error bars are lower than the marker size.

The behaviour of the measured electrical properties with temperature is in agreement with the porosity and UPV measurements. In particular, the sample thermal cracking with increasing temperature generates an increase in the rock pore volume. These voids are filled by air (acting as an electrical insulator) in dry conditions. Accordingly, the measured $\rho_{a,dry}$ progressively increases. Conversely, in wet conditions pores and voids are filled by fluid (acting as an electrical conductor). These explanation is in accordance with the Sauer et al.' theory [38] that recognized three main paths which the electrical current can take in an unsaturated porous medium:

1 Through alternating layers of rock particles and interstitial soil solution
2 Through or along the surface of the rock particles in direct contact with one another
3 Through the interstitial fluid.

Consequently, if the porous medium is saturated by saline solution, the model 3 is dominant and the ER decrease with the increase of crack density. Vice-versa, in dry conditions, the volume void is filled by air, that has effectively zero conductance: the model 1 is dominant, ER moderately increase and it depends mainly by mineral shape and crack tortuosity.

In this configuration, $\rho_{a,wet}$ progressively reduces with increasing thermal damage, since the quantity of the fluid within the pore volume significantly increases. The very low values of $\rho_{a,wet}$ at 600°C are again consistent with the decomposition processes described above and the pervasive diffusion of fluids within the rock matrix, strongly increasing the conductivity.

3.4 UCS tests

The results of UCS tests are listed in Table 2 and the complete stress-strain curves are shown in Figure 7. Results are also reported in Figure 8 as a function of the temperature treatment. The variations in σ_u are weak until a temperature of 400°C is attained (Figures 8a and 8b) with a slight increase (about 4 MPa on average) from 105 to 200°C. Then a significant drop in strength occurs from 400°C upwards that mirrors the major modifications going on within the microstructure because of mechanical softening due to incremental crack damage and approach to the calcite decomposition.

Table 2: Summary of UCS test results for each sample (first column of σ_u, E_s, E_t, E_{av}, ν and G) and average for each sample class (second column of σ_u, E_s, E_t, E_{av}, ν and G).

Thermal treatment	**Sample**	**σ_u [MPa]**		**E_s [GPa]**		**E_t [GPa]**		**E_{av} [GPa]**		**ν**		**G [GPa]**	
T105	VA_C01	107	110	129	122	114	123	115	113	0.38	0.39	47	44
	VA_C02	107		103		126		98		0.43		36	
	VA_C03	117		132		129		125		0.37		48	
T200	VA_C04	118	114	69	74	97	99	97	95	0.26	0.26	27	29
	VA_C05	113		77		100		95		0.28		30	
	VA_C06	110		75		99		94		0.22		31	
T400	VA_C07	89	103	24	30	71	72	65	65	-0.05	-0.003	13	15
	VA_C08	111		33		76		68		0.004		16	
	VA_C09	107		33		68		62		0.04		16	
T600	VA_C10	85	80	9	11	29	33	27	29	0.02	0.065	5	5
	VA_C11	76		12		37		31		0.11		6	

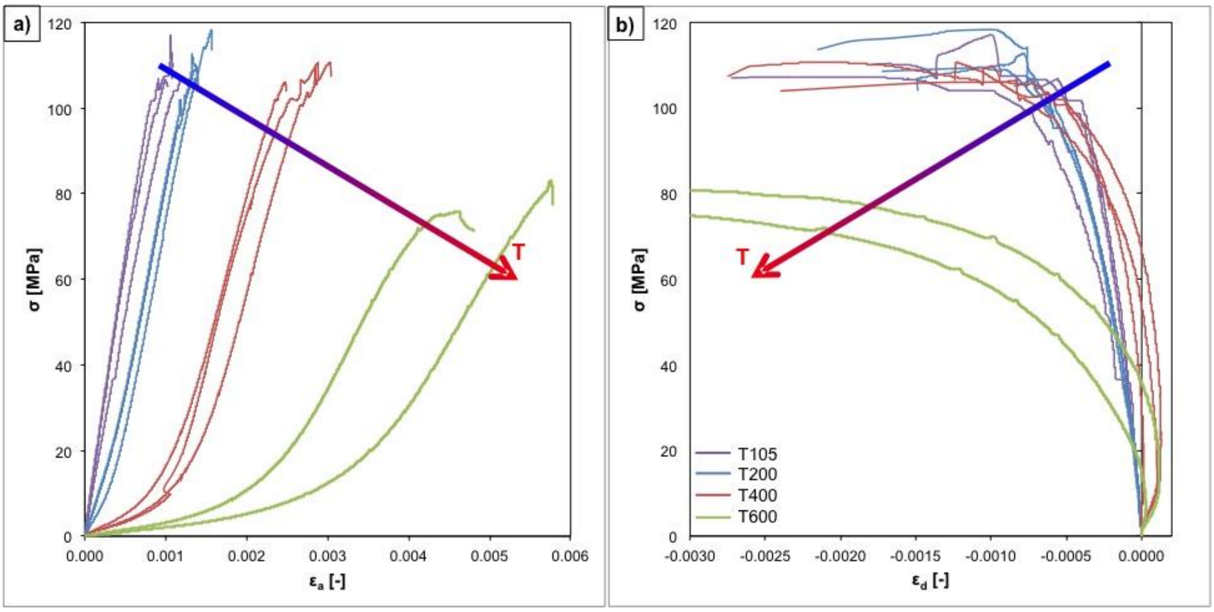

Figure 7: (a) Marble axial and (b) diametric stress-strain curves. The arrow represents the increase of heating temperature.

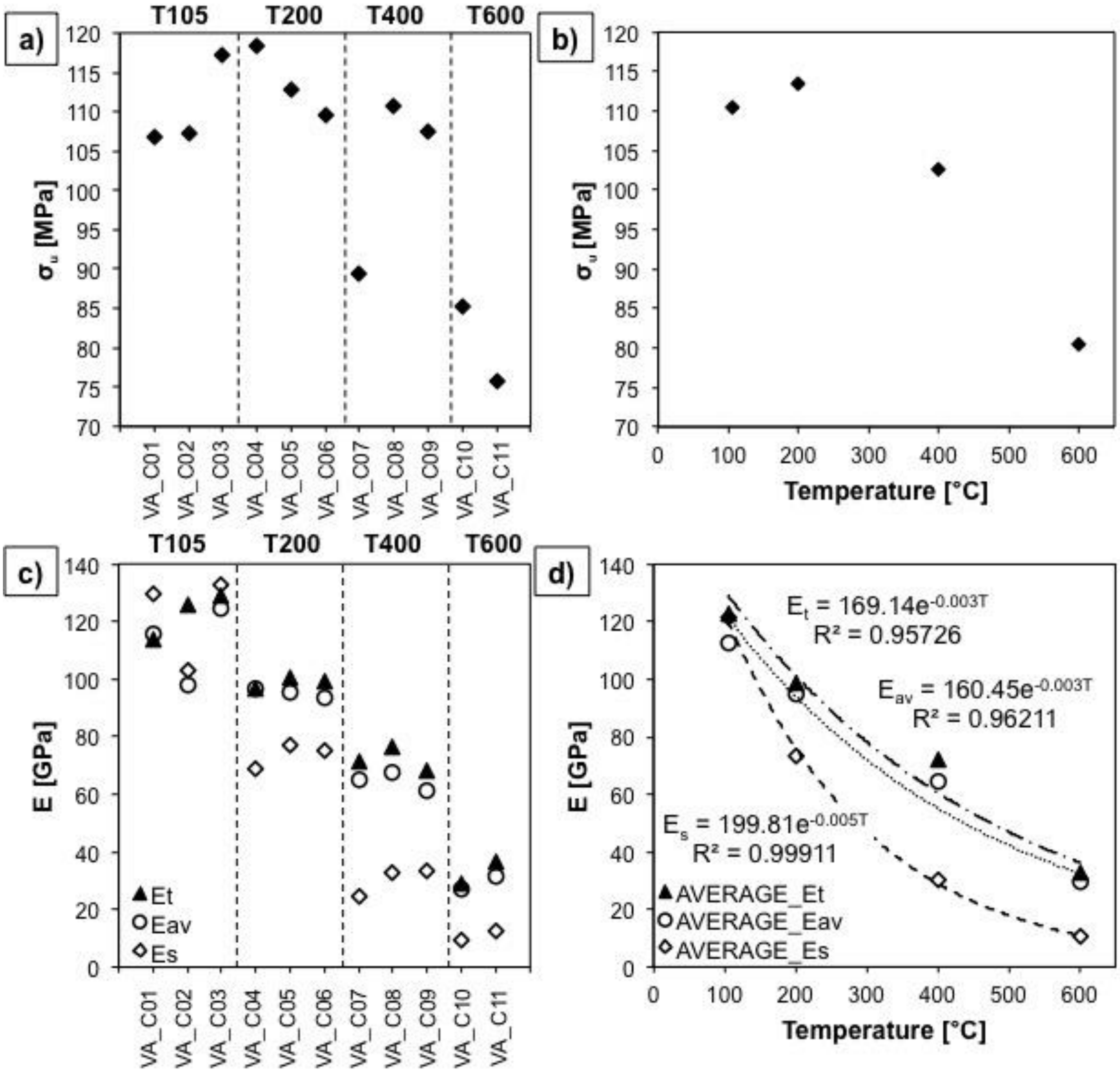

Figure 8: (a) UCS values measured on each sample. (b) Relationships between the average UCS of each sample class (T105 to T600) and the target temperature. (c) Tangent (triangles), average (circles) and secant (diamonds) Young's moduli for each sample after thermal treating. (d) Relationship between the average values of Young's moduli for each sample class and temperature.

The Young's moduli (E_s, E_t and E_{av}) accordingly progressively decrease with respect to the temperature increase. As shown in Figure 8d, the drop in E_s is more significant compared to both E_t and E_{av}. Exponential relationships between elastic moduli and temperature were found:

$$E_s = 199.81e^{-0.005T} \qquad (12)$$

$$E_t = 169.14e^{-0.003T} \qquad (13)$$

$$E_{av} = 160.45e^{-0.003T} \qquad (14)$$

with R^2 of 0.999, 0.957 and 0.962 respectively.

The differences between the trend of E_s and E_t-E_{av} can be also explained by analysing the stress-strain curve in Figure 7a where it is clear how the non-linearity in the initial deformation phase increases as function of temperature. From 400°C target temperature, the samples also showed a peculiar behaviour: the sign of diametric strain at the beginning of the tests was opposite to the normal, indicating sample expansion and not sample contraction. This behaviour was observed for each sample that belongs to T400 and T600 classes but is more marked for the T600 class (see Figure 7b). This is an independent evidence of the major changes occurring within the rock matrix bringing the sample to a more ‘ductile’ behaviour, which generates a sample expansion compared to the contraction observed at lower temperatures driven from elastic processes typical of the brittle behaviour. In order to verify that the anomalous sign in diametric strain was neither an effect of surface, nor of the strain gauges, the UCS test on sample VA_C08 was performed with an imposed diametric strain rate of -1 μm/s. For satisfying this constrain, the sample was subjected to an instantaneous load of about 60 MPa, indicating that up to that stress level sample expansion is still expected.

This effect results in negative or near zero average Poisson’s ratios (see Table 2). The progressive reduction of Poisson's ratio with temperature is coherent with what observed by means of UPV measurements.

3.5 Microscopic observations

Photomicrographs of some thin sections treated at different temperature levels are shown in Figure 9. Only thin sections perpendicular (⊥) to the sample bedding are shown as they better display the damage developed within the samples, particularly in terms of crack damage.

In general all the reported images show the sample structure as constituted by a relatively homogeneous grain size with finer-grained (up to 0.15 mm) isotropic and interlobate aggregate of calcite. A weak preferred dimensional orientation of the slightly elongate crystals and parallel clusters of coarser-grained crystals of calcite (up to 0.4 mm long) can also be observed. These observations are coherent with the expected sample bedding.

From 400°C set temperature (Figure 9c), crack damages appear to be evident within this general structure. Particularly, in Sample T600 (Figure 9d) sparse, but major fractures are visible. These are oriented parallel to the sample anisotropy, and spatially associated with the boundaries between the finer-grained matrix and the clusters of calcite. A clear weakness fracture band is also evident in this sample.

These microscopic observations well indicate the progressive development of significant crack damage within the samples from 400°C. A more marked increase in fractures is evident particularly at 600 °C coherently with the calcite decomposition processes which enhance fracture formation and propagation and in agreement with the measured reduction of mechanical parameters within this range.

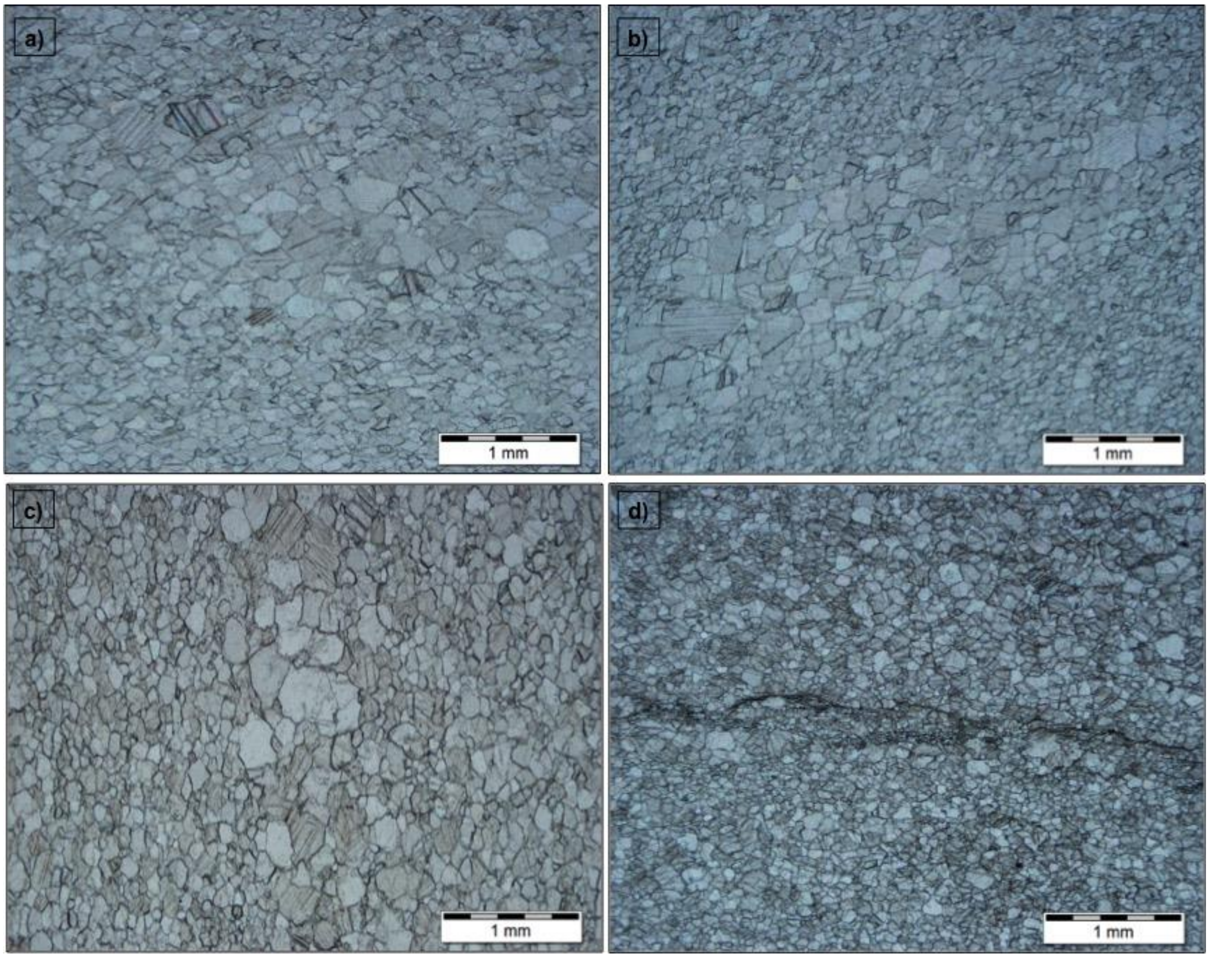

Figure 9. Photomicrograph of five thin sections at room temperature (a) and threated at 200°C (b), 400°C (c) and 600 °C (d). In (d), a clear crack was developed along the main anisotropy.

4. Towards an Unified Damage Indicator

This study has highlighted a degradation of the mechanical parameters with respect each step of temperature applied and mirrored by all physical parameters measured. An exponential trend is observed, driven specifically by the behaviour at temperatures above 400 °C, where thermo-chemical reactions enhance significantly the crack damage formation and propagation increasing the bulk porosity. Several authors have calculated exponential relationships between physical parameters and temperature. For instance, Dwivedi et al. [9], in their study on salt rocks, found an exponential relation between ultrasonic pulse velocity and temperature

$$V_P = 3380e^{-0.0032T} \qquad (15)$$

that is in good agreement with the one proposed here, especially regarding the exponential value.

On the contrary, Liu et al. [39] performing post-high-temperature experiments on granite and sandstone specimens proposed linear relationships between P-wave velocity and temperature as follow

$$V_{P,Granite} = 4700.167 - 4.608T \qquad (16)$$

$$V_{P,Sandstone} = 2018.988 - 1.569T \qquad (17)$$

The same linear regression was found for Young’s modulus

$$E_{Granite} = 37.092 - 32.160\left(\frac{T}{1000}\right) \quad (18)$$

$$E_{Sandstone} = 21.262 - 14.210\left(\frac{T}{1000}\right) \quad (19)$$

The authors [39] stated that physical and mechanical parameters after high-temperature treatment all exhibit similar variation with temperature, showing a linear inverse dependence for each parameter. Neglecting the interpolation law, in the present study the same behaviour has been observed:

Zhao et al. [10], performing triaxial tests on coal and granite samples under high temperature and high-pressure conditions, presented exponential relationships between Young's modulus and temperature which show a similar trend to the one reported in this work and again very similar exponential values.

$$E(coal) = 19.6e^{-0.005T} - 1.55 \quad (20)$$

$$E(granite) = 60e^{-0.006T} \quad (21)$$

These results were obtained at "in-situ" high temperature conditions and with limited measurements of physical parameters. Thus the integrated methodology of several physical and mechanical parameters "pre" and "post" thermal treatment described in this paper is a reliable tool for studying the temperature effects due to multiple cycles of heating and their effects on a variety of parameters.

In support of the findings reported in this paper, seismic velocities exponential relationships are well recognized in literature [e.g. 40] between both V_P and V_S and porosity. These relationships have the form:

$$V_{P,S} = V_{0\,P,S}e^{-c\,n} \quad (22)$$

where V_0 is a reference velocity value, n is the porosity and c is a fitting parameter. The reference velocity value is known to depend on the mineralogical composition of the sample and is considered constant in geomaterials having the same composition. The fitting parameter instead depends on the rock texture and can vary depending on the specific rock formation process. In the presented experiments, it has been observed that the thermal effect is directly correlated to the porosity (Figure 4d), which results to be the key parameter for analysing the incremental damage induced by the thermal treatment. Moreover, these porosity relationships are due to the increased crack density due to thermal degradation induced by the heating and cooling stages. Particularly above 400 °C the inferred increase of crack density can be observed by optical observations: Figure 9d shows the development of a pervasive system of fractures along a weakness plane parallel to the principal anisotropy direction. Thermal expansion and contraction along with decomposition processes can induce diffuse microcracking that eventually localise along macro fractures that develop along the texturally favourable orientations.

Since the porosity variation is intimately linked to the formation and propagation of fracture, we can therefore use porosity as the most quantitative indicator of the thermally induced damage, which we define as D_n. Based on Equation 7, it is possible to quantify D_n of the tested specimens as follows:

$$D_n = 1 - \frac{n_{RT}}{n(T)} \quad (23)$$

where n_{RT} is the room-temperature porosity and $n(T)$ is the porosity evaluated at the different target temperatures. D_n can assume values ranging from 0 to 1 (Figure 10): when it is 0 there are no effects of temperature on the sample porosity. Vice versa, when it is 1 the damage is so diffused that the rock loses cohesion. It should be noted that for the tested specimens, at 600 °C, the value of D_n is 0.94. Thus, the considered rock is close to total thermal damage.

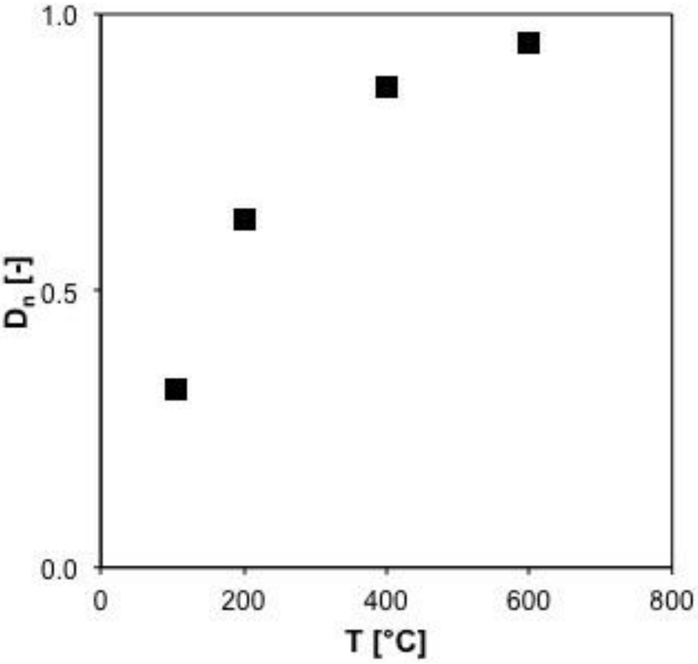

Figure 10: Thermal damage, D_n, vs temperature.

Given that the observed thermal degradation effect on the rock samples is mainly driven by changes in porosity we therefore suggest that a formulation like equation 15 can exist relating the temperature and other physical properties, such as seismic velocities and electrical resistivity, for which the porosity influence result to be relevant. Determined empirical relationships with porosity, shown in Figure 11a and Figure 11b for UPV and electrical resistivity respectively, follow:

$$n = 76652{V_P}^{-1.439} \qquad (24)$$

$$n = 174326{V_S}^{-1.631} \qquad (25)$$

$$n = 0.08F^{-0.55} \qquad (26)$$

where F is the formation factor, expressed as the ratio between $\rho_{a,wet}$ and the fluid resistivity. These relationships have a very high R^2, of 0.981, 0.983 and 0.90, confirming the strong dependence of the measured parameters on the rock porosity.

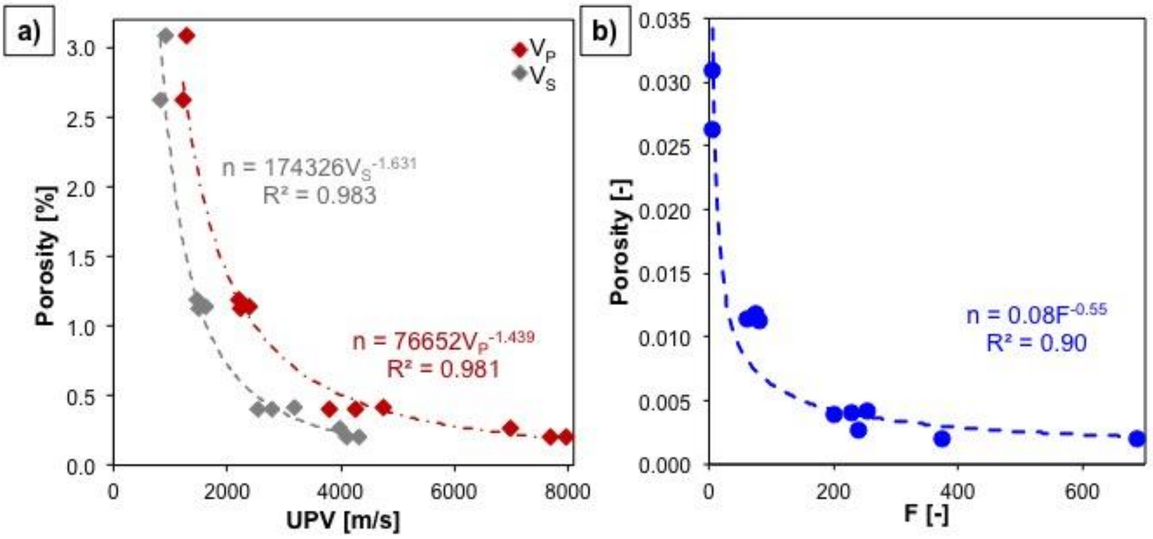

Figure 11: Empirical relationships for porosity estimation from (a) P- and S-wave ultrasonic pulse velocities, (b) wet electrical resistivity (measured on saturated samples).

Therefore the proposed thermal degradation relationship can assume the form:

$$P(T) = P_0 A(T) \qquad (27)$$

where *P(T)* is the considered physical parameter, *P_0* its mineralogical reference value and A(T) is a function, dependent on temperature T. As previously shown, in scientific literature there are many relationships based on this model [9, 10, 39, 40]. The function A(T) should comply with these requirements: firstly, P_0 should be constant in lithology with the same mineralogy and secondly, it should be convenient to assume that A(T) tends to 1 when T is close to room temperature. Both prescriptions can be fulfilled if A(T) follow an exponential law and consequently equation 27 can be rewritten as :

$$P(T) = P_0 e^{-cT} \qquad (28)$$

where c is the fitting parameter dependent on the specific rock structure.

In the present work we propose in equations 8 to 14 these two last calibrating factors for the tested rock. Similar calibration procedures could be undertaken for different rock types to allow for a precise quantification of the thermal degradation effect.

Despite this well-defined behaviour on the measured physical parameters, σ_u is observed to follow a different trend. Indeed, a moderate increase of σ_u is observed till a certain temperature level. Analysing the stress-strain curves of Figure 7a, T200 specimens mark, for the tested marble, this turning point. Accordingly, to other authors [20-24], during UCS tests, due to crack closing and grain rearrangements there is a densification stage that, from one side increases the axial deformation (as expected) but on the other side increases the axial strength.

UCS tests also showed other two interesting behaviours: the first one is the non-linearity in the initial deformation phase (Figure 7a) that is direct consequence of the anelasticity due to the increase of the amount of microcracks generated by thermal treatment in the specimens.

The second is the negative value of Poisson's ratio for T400 and T600 specimens. For isotropic materials, the elasticity theory imposes that E shall be greater than 0 and ν varying between -1 and 0.5. Thus, theoretically, negative values of ν are allowed. However, in experimental tests ν always results positive for real isotropic material.

The most plausible explanation for negative values of ν is the existence of residual stresses induced by the thermal cycles (presumably during cooling). The rise in temperature increases the crack density and lead to the weakening or even loss of grain boundary bonds, eventually producing unconsolidated material that under stress is mobilized plastically and flows along the sample.

The combined measurement of both P- and S-wave velocities offers the opportunity to retrieve low-deformation (initial deformation phase of strain-stress curve) mechanical parameters (E, G and ν) from indirect and non-destructive tests, following:

$$G = \rho V_S^2 \qquad (28)$$

$$\nu = \frac{V_P^2 - 2V_S^2}{2(V_P^2 - V_S^2)} \qquad (29)$$

$$E = 2G(1 + \nu) \qquad (30)$$

E, G and ν values from UCS tests were evaluated at an axial load of 10 MPa and considering the correspondent values of axial and diametric strain.

In Table 3, the results of the E, G and ν values estimated from UPVs and derived from UCS tests are listed. The general trend of the investigated parameters agrees with the previous observations: increasing the temperature, there is a drop in mechanical properties for both estimated and measured ones. The error in the estimation is quantifiable in less than 10% on average. The main differences concern the negative values of Poisson's ratio for the classes T400 and T600. Since V_P cannot be lower than V_S, Equation 21 can never return negative results.

Table 3: Comparison between low-deformation mechanical parameters (E, ν and G) evaluated from UCS tests and UPV measurements.

Thermal treatment	**Sample**	**E_{10MPa} [GPa]**		**E_{UPV} [GPa]**		**ν_{10MPa}**		**ν_{UPV}**		**G_{10MPa} [GPa]**		**G_{UPV} [GPa]**	
T105	VA_C01	135	129	119	119	0.26	0.24	0.30	0.28	54	52	46	46
	VA_C02	110		108		0.18		0.26		47		43	
	VA_C03	143		131		0.28		0.29		56		51	
T200	VA_C04	36	51	38	48	0.07	0.10	0.10	0.11	17	23	17	22
	VA_C05	60		60		0.10		0.09		27		27	
	VA_C06	57		47		0.15		0.13		25		21	
T400	VA_C07	10	11	13	14	-0.09	-0.07	0.10	0.09	5	6	6	6
	VA_C08	11		13		-0.11		0.08		6		6	
	VA_C09	13		15		-0.01		0.08		6		7	
T600	VA_C10	4	4	4	4	-0.04	-0.03	0.09	0.05	2	2	2	2
	VA_C11	5		4		-0.01		0.01		3		2	

5. Conclusions

Temperature is a key parameter for modelling many geological engineering applications (deep drilling, geothermal energy exploitation, nuclear waste disposal, CO2 storage etc.) since it has a significant influence on physical and mechanical properties of rocks. However, since each rock type has a different behaviour after thermal treatment, it is important to develop dedicated studies and calibrated equations for each lithology.

In this paper, a series of laboratory tests on an Italian marble was performed for investigating the variation of the rock physical behaviour as a function of temperature. Several parameters (ρ, n,V_P and V_S, ρ_a, σ_u) were measured on core samples subjected to four different target temperatures (105, 200, 400 and 600°C). Microscopic observations on thin sections were analyzed to evaluate the heating/cooling effects on marble microstructures.

For the analysed rock, the range of temperatures from 200 to 400°C marks a turning point in the trend of physical and mechanical characteristics: up to 200°C, all the considered parameters are not significantly sensitive to the temperature. Indeed, the axial strength shows a moderate increase (about 4 MPa) despite the axial deformation increases. This behaviour might be associated with compaction due to the closure of intergranular cracking that are not completely linked. Even if this aspect is not so evident by analysing thin sections due to some limitations in their preparation procedure, this hypothesis can be supported by analysing the trend of F values. At 400°C, there is a significant drop in ρ, V_P and V_S, F, σ_u and E values and an increase in n. The presence of intragranular cracks and the high intergranular crack density are the leading parameters of this degradation.

The previous observations suggest that n can be considered the most sensitive parameter with temperature. Thus, the authors proposed the coefficient D_n for measuring the thermal damage of rocks. If D_n is close to 0, it means that the effects of temperature on the rock sample can be neglected; vice-versa, if it is close to 1, the sample has undergone irreversible degradation.

Finally, it is important to underline the exponential dependence of physical and mechanical parameters with temperature for the studied marble rock. This dependence was already observed in other works for other rock types [9, 10, 26]. Future works should be done for verifying this trend.

A remark must be made on the size of the sample to be representative: since macroscopically and microscopically the tested marble doesn't show a relevant heterogeneity (as also confirmed by the low variability in the measurements between samples of the same group), the authors considered the number of specimens sufficient for providing reliable and representative results. However, this aspect shall be taken into account if other lithologies will be considered in future works.

Since in many geo-engineering applications the temperature is coupled with pressure, it will be interesting to investigate the effects of the latter on rock characteristics, especially if the proposed relationships are applicable or they should be modified.

Another aspect that will require further analyses is the observation of negative Poisson's ratio at high temperature: in particular it will be interesting to investigate the reasons of this behaviour and if it occurs in other lithotypes.

Conflicts of Interest

The authors declare that there is no conflict of interest regarding the publication of this paper.

Acknowledgements

Special acknowledgements should be given to Carbocalcio Cuneese S.p.A that agrees the use of its materials for observation, sampling and laboratory tests.

Funding Statement

This project has received funding from the European Union's Horizon 2020 research and innovation programme under the grant agreement No. 727550.

References

[1] Homand-Etienne F and Houpert R. Thermally induced microcracking in granites: characterization and analysis. *Int. J. Rock. Mech. Min. Sci. & Geomech. Abstr*. 1989;26;2:125-134.

[2] Castagna A, Ougier-Simonin A, Benson PM et al. Thermal Damage and Pore Pressure Effects on Brittle-Ductile Transition of Comiso Limestone. *Journal of Geophysical Research – Solid Earth*, in press.

[3] Gomez-Heras M, McCabe S, Smith, Bernard BJ, Fort R. Impacts of Fire on Stone-Built Heritage An Overview. *Journal of Architectural Conservation*. 2009;15:47-58. doi:10.1080/13556207.2009.10785047.

[4] Giuliani A and Fornaro M. Criteri geologico applicativi per il reperimento di materiali lapidei originari per il restauro della Cappella della SS. Sindone (Torino, NW Italia). *VIII Convegno Nazionale dei Giovani Ricercatori di Geologia Applicata*. 2010:86-89.

[5] Koca MY, Ozden G, Yavuz AB et al. Changes in the engineering properties of marble in fire-exposed columns. *Int. J. Rock Mech. Min. Sci*. 2006;43:520–530.

[6] Yavuz AB, Topal T. Thermal and salt crystallization effects on marble deterioration: Examples from Western Anatolia, Turkey. *Eng. Geo*. 2007;90:30-40.

[7] Rutter EH. The influence of temperature, strain rate and interstitial water in the experimental deformation of calcite rocks. *Tectonophysics*. 1974;22:311-334.

[8] Jansen DP, Carlson SR, Young RP, Hutchins DA. Ultrasonic-imaging and acoustic-emission monitoring of thermally-induced microcracks in lac-du-bonnet-granite. *J. of Geophys. Res. Sol. Earth*. 1993;98:22231-22243.

[9] Dwivedi RD, Goel RK, Prasad VVR, Sinha A. Thermo-mechanical properties of Indian and other granites. *Int. J. Rock Mech. Min. Sci*. 2008;45;3:303-315.

[10] Zhao Y, Wan Z, Feng Z, Yang D, Zhang Y, Qu F. Triaxial compression system for rock testing under high temperature and high pressure. *Int. J. Rock Mech. Min. Sci*., vol. 52, pp. 132-138, 2012.

[11] Tullis J and Yund RA. Experimental deformation of dry Westerly granite. *J. Geophys. Res.* 1977;82:5705-5718.

[12] Wong TF. Effects of temperature and pressure on failure and post-failure behavior of Westerly granite. *Mech. Mater*. 1982;1:3-17.

[13] David C, Menéndez C, Darot M. Influence of stress-induced and thermal cracking on physical properties and microstructure of La Peyratte granite. *Int. J. Rock. Mech. Min. Sci.* 1999;36;4:433-448.

[14] Chaki S, Takarli M, Agbodjan WP. Influence of thermal damage on physical properties of a granite rock: porosity, permeability and ultrasonic wave evolutions. *Constr. Build. Mater.* 2008;22;7:1456–1461.

[15] Chen YL, Ni J, Shao W, Azzam R. Experimental study on the influence of temperature on the mechanical properties of granite under uni-axial compression and fatigue loading. *Int. J. Rock. Mech. Min. Sci.* 2012;56;8:62-66.

[16] Liu S and Xu J. Mechanical properties of Qinling biotite granite after high temperature treatment. *Int. J. Rock. Mech. Min. Sci.* 2014;71:188-193.

[17] Yin T, Li X, Cao W et al. Effects of Thermal Treatment on Tensile Strength of Laurentian Granite Using Brazilian Test. *Rock. Mech. Rock Eng.* 2015;48:2213-2223.

[18] Chen YL, Wang SR, Ni J, Azzam R, Fernández-steeger TM. An experimental study of the mechanical properties of granite after high temperature exposure based on mineral characteristics. *Eng. Geol*. 2017;220:234-242.

[19] Peng J, Rong G, Cai M, Yao MD, Zhou CB. Physical and mechanical behaviours of a thermal-damaged coarse marble under uniaxial compression. *Eng. Geol.* 2016;200:88-93.

[20] Ferrero AM and Marini P. Experimental Studies on the mechanical behaviour of two thermal cracked marbles. *Rock Mech. Rock Eng.* 2000;34;1:57-66.

[21] Lion M, Skoczylas F, Ledésert B. Effects of heating on the hydraulic and poroelastic properties of bourgogne limestone. *Int. J. Rock. Mech. Min. Sci.* 2005;42;4:508-520.

[22] Malaga-Starzec K, Åkesson U, Lindqvist JE, Schouenborg B. Microscopic and macroscopic characterization of the porosity of marble as a function of temperature and impregnation. *Constr. Build. Mater.* 2006.

[23] Yavuz H, Dermirdag S, Caran S. Thermal effect on the physical properties of carbonate rocks. *Int. J. Rock. Mech. Min. Sci.* 2010;1:94-103.

[24] Gonzalez-Gomez WS, Quintana P, May-Pat A, Avilés F, May-Crespo J, Alvarado-Gil JJ. Thermal effects on the physical properties of limestones from the Yucatan Peninsula. *Int. J. Rock Mech. Min. Sci.* 2015;75;182-189.

[25] Liang WG, Xu SG, Zhao YS. Experimental study of temperature effects on physical and mechanical characteristics of salt rock. *Rock Mech. Rock Eng.* 2006;39;5:469-482.

[26] Ranjith PG, Viete DR, Chen BJ, Perera MSA. Transformation plasticity and the effect of temperature on the mechanical behaviour of Hawkesbury sandstone at atmospheric pressure. *Eng. Geol.* 2012;151:120-127.

[27] Ding QL, Ju F, Mao XB, Ma D, Yu BY. Song SB. Experimental investigation of the mechanical behaviour in unloading conditions of sandstone after high-temperature treatment. *Rock Mech. Rock Eng.* 2016;49;7:2641-2653.

[28] Sun Q, Chen S, Gao Q, Zhang W, Geng J, Zhang Y. Analyses of the factors influencing sandstone thermal conductivity. Acta Geodyn. Geomater., vol. 2, no. 186, pp. 172–180, 2017.

[29] Brotóns V, Tomás R, Ivorra S, Alarcón JC. Temperature influence on the physical and mechanical properties of a porous rock: San Julian's calcarenite. *Eng. Geol*. 2013;167:117-127.

[30] Bakker R, Violay M, Benson P, Vinciguerra S. Ductile flow in sub-volcanic carbonate basement as the main control for edifice stability: New experimental insights. *Earth and Planetary Science Letters*. 2015; 430:533-541.

[31] IMAGE-D3.03. Physical properties of rock at reservoir conditions. Integrated Methods for Advanced Geothermal Exploration. Collaborative Project – GA No. 608553. 2016:1-70.

[32] Carraro F, Dal Piaz GV, Franceschetti B, Malaroda R, Sturani C, Zanella E. Note illustrative della Carta Geologica del Massiccio dell'Argentera alla scala 1:50.000. *Memorie della Società Geologica Italiana*. 1970;9:557–663 (in Italian).

[33] Barale L, Bertok C, d'Atri A, Martire L, Piana F, Domini G. Geology of the Entracque–Colle di Tenda area (Maritime Alps, NW Italy). *Journal of Maps*. 2016;12;2:359-370.

[34] ISRM. Suggested methods for determining water content, porosity, density, absorption and related properties and swelling and slake-durability index properties. 1977.

[35] ASTM D2845-08. Standard Test Method for Laboratory Determination of Pulse Velocities and Ultrasonic Elastic Constants of Rock," ASTM, International (American Society for Testing and Materials), West Conshohocken, Pennsylvania, USA. 2008.

[36] Clement R, Bergeron M, Moreau S. COMSOL Multiphysics modelling for measurement device of electrical resistivity in laboratory test cell. *Proceedings of the 2011 COMSOL Conference in Stuttgart*. 2011.

[37] ISRM. Suggested methods for determining the uniaxial compressive strength and deformability of rock materials. 1977.

[38] Sauer MCJr, Southwick PE, Spiegler KS, Wyllie MRJ. Electrical conductance of porous plugs: Ion exchange resin-solution system. *Ind. Eng. Chem*. 1955;47:2187-2193.

[39] Liu S, Xu J. An experimental study on the physico-mechanical properties of two post-high-temperature rocks. *Eng. Geo*. 2015;185:63–70.

[40] Musso G, Cosentini RM, Foti S, Comina C, Capasso G. Assessment of the structural representativeness of sample data sets for the mechanical characterization of deep formations. *Geophysics*, 2015;80:441-457.